PHYSICAL REVIEW C **82**, 061306(R) (2010)

Correlations of experimental isotope shifts with spectroscopic and mass observables

R. B. Cakirli,[1,2] R. F. Casten,[3] and K. Blaum[1,4]

[1]*Max-Planck-Institut für Kernphysik, Saupfercheckweg 1, D-69117 Heidelberg, Germany*

[2]*Department of Physics, University of Istanbul, Istanbul, Turkey*

[3]*Wright Nuclear Structure Laboratory, Yale University, New Haven, Connecticut 06520, USA*

[4]*Physikalisches Institut, Ruprecht-Karls-Universität Heidelberg, Philosophenweg 12, D-69120 Heidelberg, Germany*

(Received 19 June 2010; published 17 December 2010)

Experimental differential observables relating to mean square charge radii, spectroscopic, and mass observables of even-even nuclei are presented for different regions in the nuclear chart. They exhibit remarkable correlations, not heretofore recognized, that provide a new perspective on structural evolution, especially in exotic nuclei. This can also be a guide for future measurements of charge radii, spectroscopic observables, and masses, as well as for future theoretical approaches.

DOI: 10.1103/PhysRevC.82.061306 PACS number(s): 21.10.Ft, 21.10.Dr

One of the scientific opportunities associated with nuclei far from stability is to study the evolution of structure with nucleon number in regions of the nuclear chart never before accessible. This will contribute toward a comprehensive understanding of nuclei, but it also presents a challenge because of the minimal data that will often be available, especially at the extremes of accessibility. Therefore, just as it is essential to construct the facilities and instruments to access exotic nuclei, it is also critical to develop new approaches to extract the most physics from limited data. This Rapid Communication presents a new way of looking at nuclear structure and structural evolution to identify heretofore unrecognized, yet pervasive, correlations among a broad range of observables.

Complex many-body systems in a variety of physical systems display properties that reflect either the behavior of their microscopic ingredients or the symmetries and correlations of the system itself. Such many-body systems typically exhibit several common categories of properties—binding energy, collective correlations, transition rates, and often, observables that relate to their geometric shape or symmetry structure. Nuclei provide an especially intriguing opportunity for such studies. Although they share the existence of regularities in common with other many-body systems, nuclei differ because they contain two kinds of particles and experience both the strong and Coulomb forces. Moreover, the regularities they exhibit—arising primarily from the short-range nature of the nuclear force and the Pauli principle—appear both in individual nuclei and across the nuclear chart. Thus the experimental ability to study both the ground and excited states of individual nuclei, as well as to vary the number of interacting "bodies" (nucleons), is a special opportunity.

It is the purpose of this Rapid Communication to examine and compare several observables that elucidate nuclear structure and its evolution with N and Z. These observables probe a variety of structural features—individual nucleonic motion, collective phenomena, and integral properties. When looked at over a range of nuclei, their behavior appears quite different. We will show, however, that an alternate way of considering them reveals remarkable correlations that present a unified view of this structural evolution and that have applications to the study of exotic nuclei. The essential step will be to focus on correlations of *differential observables*, that is, on differences of these observables from one nucleus to the next. To our knowledge, the generality and pervasiveness of these correlations have not hitherto been recognized before. Furthermore, they were *a priori* unexpected in the sense that, prior to this work, no one had proposed that such correlations might apply (although, piecemeal, individual examples have been discussed in specific situations). Of course, once exhibited, as we do here, it is possible to go back to the individual observables and see why the differential observables behave as they do.

To present these results, we will use familiar observables in well-studied regions whose general behavior is well known to illustrate our findings. However, their main application, as noted, will likely be in new regions with sparse data. These results are of interest from five perspectives: The similarity in the behavior of the differential observables despite the apparent differences in the observables themselves; the pervasiveness of the correlations; the ability to use values of one or two of these observables in new regions to infer approximate values of others—both to determine structure and structural evolution and to guide further experiments; their use in amplifying deviant behavior; and, as a challenge to theory, perhaps leading to new insights into the structure of these systems.

We start with the rare-earth region. The top panel of Fig. 1 (left) shows the mean square charge radii $\langle r^2 \rangle$ against neutron number (N) for the rare-earth region. Charge radii generally increase with nucleon number, with sharp rises when deformation sets in (here at $N \sim 90$). The lower rows of Fig. 1 (left) present data for four other nuclear ground and excited state observables, namely, the excitation energy of the first excited 2^+ state [$E(2_1^+)$], the energy ratio of the energies of the first 4^+ and the first 2^+ excited states [$R_{4/2}$], the transition probability between the first 2^+ and the 0^+ ground state [$B(E2 : 2_1^+ \rightarrow 0_1^+)$], and two-neutron separation energies [S_{2n}]. They all exhibit familiar behavior at closed shells and at the onset of deformation. $E(2_1^+)$ peaks at magic numbers and drops at the onset of deformation. The ratio $R_{4/2}$ is <2 for nuclei very near magic numbers, $R_{4/2} \sim 2.0$–2.4 in vibrational nuclei and $R_{4/2} \sim 3.33$ in well-deformed rotors. The $B(E2 : 2_1^+ \rightarrow 0_1^+)$ values have a similar behavior as $R_{4/2}$

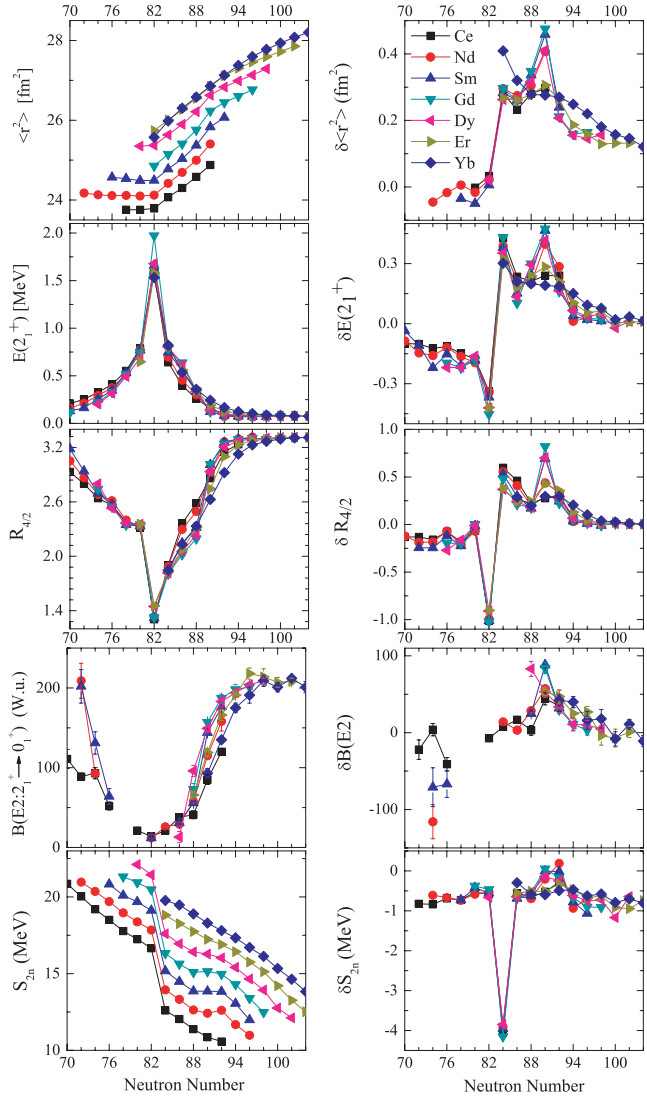

FIG. 1. (Color online) (Left): Experimental $\langle r^2\rangle$, $E(2_1^+)$, $R_{4/2}$, $B(E2:2_1^+\rightarrow 0_1^+)$, and S_{2n} values with $N = 70$–104 [1,2]. (Right): Differential values of these observables defined by $\delta\langle r^2\rangle(N) = \langle r^2\rangle_N - \langle r^2\rangle_{(N-2)}$, $\delta E(2_1^+)(N) = (E_{(N-2)} - E_N)/(E_{(N-2)} + E_N)$, $\delta R_{4/2}(N) = R_N - R_{(N-2)}$, $\delta B(E2:2_1^+\rightarrow 0_1^+)(N) = B(E2)_N - B(E2)_{(N-2)}$, $\delta S_{2n}(N) = S_N - S_{(N-2)}$. Note that the definition of $\delta E(2_1^+)$ is inverted in N and $(N-2)$ since its overall trendline is opposite to most of the other observables. Error bars are shown only if larger than the symbols. Large errors only occur for a few $\delta B(E2)$ values: to avoid cluttering the plots with essentially content-free points, we omitted cases (five in total in Figs. 1 and 2) where the error in $\delta B(E2) > 50\%$ and >20 W.u. In the single, important case of ^{98}Zr, whose $B(E2)$ value gives $\delta B(E2)$ values for ^{98,100} Zr, we used the Grodzins rule [3] to estimate the $B(E2)$ value, giving it a conservative uncertainty of $\pm 100\%$.

although their rise does not saturate at the onset of deformation but continues to midshell. Finally, S_{2n} values show a rapid drop immediately after a closed shell since the valence nucleons occupy less bound orbits in a newly open shell, and also exhibit a flattening in the shape transition region as energy is gained by the onset of deformation [4].

Clearly, the patterns in Fig. 1 (left) are very different from each other even though some of these observables are related [e.g., $E(2_1^+)$, $B(E2)$] via the Grodzins relation [3], and $\langle r^2\rangle$ and $B(E2)$ values through the deformation [5–8]. However, if the data are presented in terms of *isotopic differences* for adjacent (even) neutron numbers, a remarkable set of correlations among all five observables emerges, as shown in Fig. 1 (right). It should not be surprising that differential quantities can highlight physics or physical effects not easily seen otherwise. Backbending is a well-known example. Here the correlations appear both in the overall perspective they show as well as in subtle differences in the behavior of different isotopic chains. To our knowledge, as emphasized above, these five observables with ten different pairwise correlations [such as $\delta E(2_1^+)$ and δS_{2n}] have never been looked at and certainly not for such a large and diverse group of observables and over such extension regions of nuclei as shown in Fig. 1 (and Fig. 2).

While the correlations we will discuss are new, there have been occasional discussions of such differential observables in the past. Brix-Kopfermann plots [9] [Fig. 1 (top-right)] were frequently used in the past [5,6,10]. But, when long isotopic chains began to be measured, $\langle r^2\rangle$ data themselves were more often shown. The authors of Ref. [11] discussed the kink parameter, obtained from double differences of charge radii, the authors of Refs. [12,13] studied several of these quantities as a function of a control parameter, either $E(2_1^+)$ or the control parameter in the Interacting Boson Approximation (IBA) model, near $N = 90$ and the authors of Ref. [14] used δS_{2n} to identify shape transitional regions. In addition, some pairwise correlations of observables have also occasionally been studied (e.g., in Refs. [15,16]). Gerstenkorn noted correlations between $\delta\langle r^2\rangle$ and binding energy differentials, but limited to nuclei within four neutron (holes) of a neutron magic number and the authors of Ref. [16] used a liquid drop model to remove the average behavior of experimental radii and binding energies, showing that the residual differential quantities are correlated for nondeformed nuclei. We stress, however, that our approach is purely empirical with no model assumptions, and that it is general, regardless of structure.

We now return to further discussion of Fig. 1 (right). We note that each observable, except the $\delta B(E2)$ values, shows a sharp anomaly as the magic number $N = 82$ is crossed. In most cases the singularity consists of a sudden drop and then a rise as in $\delta E(2_1^+)$, $\delta R_{4/2}$, and δS_{2n}. For $\delta E(2_1^+)$ and $\delta R_{4/2}$, there is a zig-zag pattern crossing the closed shell since these two observables show extrema at the magic number. For δS_{2n}, the zig-zag oscillation occurs because of the sharp drop after the closed shell surrounded on both sides by linear trends with smaller slopes. For $\delta\langle r^2\rangle$, there is no initial drop, but one sees the sharp rise after the closed shell as nucleons start to occupy the next higher shell. Second, the differential observables all peak at the onset of deformation near $N = 90$ reflecting the sudden rise in $\langle r^2\rangle$, $R_{4/2}$, and $B(E2)$ values, the rise relative to the secular downtrend in S_{2n} and the drop in $E(2_1^+)$.

Beyond these general features, one can see subtleties in the correlations. The $\delta\langle r^2\rangle$ data near $N = 90$ in Fig. 1 (right) form two groups, with Nd, Sm, Gd, and Dy showing a sharp peak while Ce, Er, and Yb exhibit only a small rise. The other differential observables in Fig. 1 (right) exhibit similar

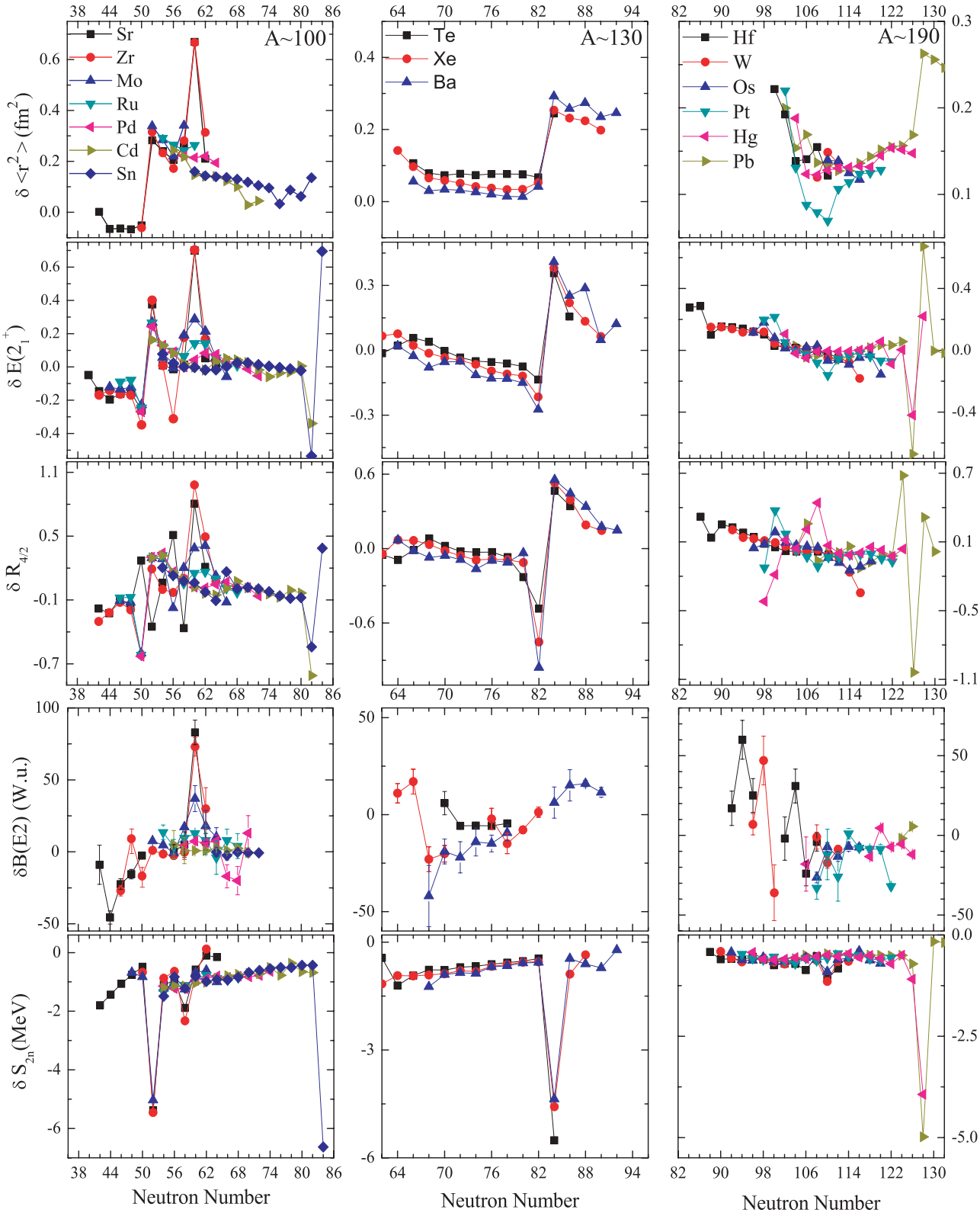

FIG. 2. (Color online) Similar to Fig. 1 but for the $A \sim 100$, 130, and 190 regions [1,2].

behavior. This is due to the more rapid onset of deformation for nuclei near $Z = 64$. Two anomalous points stand out in Fig. 1 (right): $\delta\langle r^2\rangle$ for Yb at $N = 84$ and $\delta B(E2)$ for Dy at $N = 88$. Remeasurements of both will be useful.

To check if the correlations are accidental, or specific to the rare-earth region, we present results in Fig. 2 for all other regions where sufficiently extensive data exist. The five observables in Fig. 2 show close correlations, and both

shell closures and regions of the onset of deformation (near $N \sim 60$) show similar behavior to that at $N = 82$ and $N \sim 90$, respectively, as seen in Fig. 1 (right). Once again the rapidity of the onset of deformation near $N \sim 60$ is Z dependent, being strongest in Zr and Sr, milder in Mo, and barely visible in Ru, Pd, Cd, and, of course, Sn in Fig. 2 (left). The middle and right panels show nuclei, with Z between 52 and 56, and 72 to 82 where there is no sharp onset of deformation as at $N \sim 60$ or $N \sim 90$, and this shows up consistently in the differential observables.

There are some aspects of Fig. 2 that deserve specific mention. In the $A \sim 100$ region, besides the shell closure at $N = 50$, there is a subshell closure at $N = 56$ for the Sr and Zr region [17] when the $d_{5/2}$ shell fills. In Zr this effect is particularly obvious in $\delta E(2_1^+)$ and δS_{2n}, but does not appear in $\delta\langle r^2\rangle$, $\delta R_{4/2}$, and $\delta B(E2)$. In Sr it shows up in dramatic fashion in $R_{4/2}$ where there are double oscillations at $N = 50$ and 56 that do not appear elsewhere. This is a special consequence of the shell structure relevant to Sr that is not relevant to the elements with $Z \geqslant 40$. For closed shell or closed subshell neutron numbers the lowest excited states will be largely proton excitations. Since the outermost protons in Sr fill the $f_{5/2}$ and $p_{3/2}$ orbits, proton excitations must involve occupation of the $p_{1/2}$ or higher-lying orbits. A particle-hole excitation $[p_{3/2}^{-1} \otimes p_{1/2}]$ or pair promotion from the $p_{3/2}$ orbit to the $p_{1/2}$ orbit $[(p_{3/2})^{-2} \otimes (p_{1/2})^2]$ can make a 2^+ state, but not a 4^+ state, which must involve either a pair excitation from the $f_{5/2}$ level to the $p_{1/2}$ level and a recoupling of the remaining particles in the $f_{5/2}$ orbit to $J = 4$ or an even number of excitations into the higher-lying $g_{9/2}$ orbit. Such possibilities require higher energy for 4^+ states compared to lower spin excitations. Thus, this higher energy gives an anomalous behavior for $\delta R_{4/2}$ [but not for $\delta E(2_1^+)$ or the other observables] in Fig. 2.

Last, in the $A \sim 190$ region in Fig. 2 (right), there are two clear anomalies, for Hg in the $\delta R_{4/2}$ plot and for Hf and W in the $B(E2)$ plot. The Hg effect is well understood and reflects the descent of a two-proton particle-two proton hole coexisting deformed intruder state into the low-lying spectrum [18,19]. The 4^+ states of the spherical ground band and the intruder band mix with each other and repel.

The Hf and W nuclei for $N < 106$ show strong and therefore interesting oscillations in $\delta B(E2)$. However, since incorrect experimental values appear as high-low pairs in these difference plots, remeasurements will be worthwhile. Finally, isotope shift measurements for neutron deficient nuclei in this mass region are also needed.

To close, we illustrate these ideas by data in a very different mass region, that near $Z \sim 16$. Here there are several interesting features that distinguish this region from the others we considered: breakdown of the magic numbers at $N = 20$ and 28 for certain elements, special binding effects for $N = Z$ nuclei, and much smaller shell size. In Fig. 3 we show the data for three observables, namely $E(2_1^+)$, $B(E2: 2_1^+ \rightarrow 0_1^+)$, and S_{2n} on the left and their differentials on the right. There is not enough data for $R_{4/2}$ or $\langle r^2\rangle$ to make useful plots. We recall that $\delta E(2_1^+)$ has a sharp minimum at closed shells and δS_{2n} does so just after closed shells, while $\delta B(E2)$ values are flat near magic

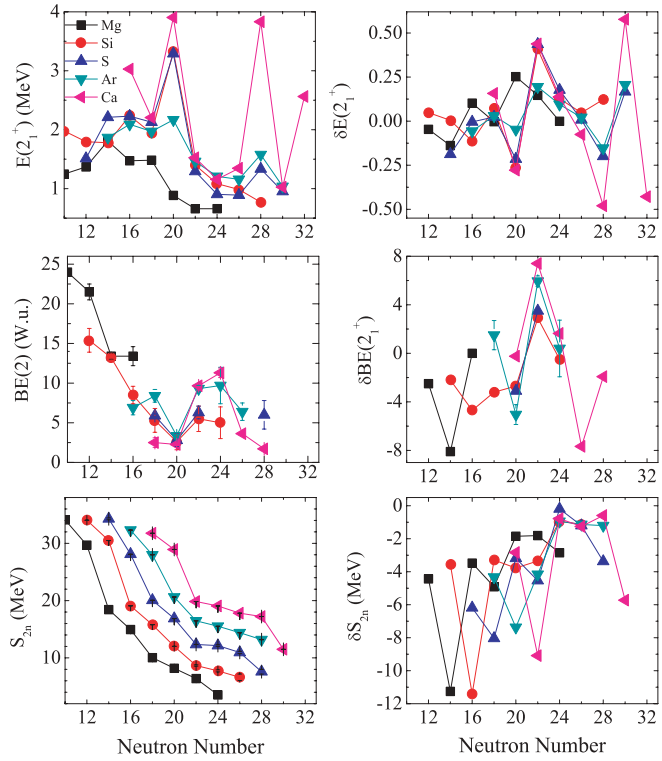

FIG. 3. (Color online) Similar to Fig. 1 but for the $A \sim 35$ region and with three observables [1,2].

numbers. All three peak either at the onset of deformation or just after (δS_{2n}). An inspection of Fig. 3 shows minima in $\delta E(2_1^+)$ at $N = 20$ for most elements, but not for Mg (as is well known [20]) and a range of behavior at $N = 28$. The lack of minima, or weak minima, at these neutrons numbers reflects the well-known breakdown of neutron magicity as a function of neutron number in this mass region. Peaks in $\delta E(2_1^+)$ and $\delta B(E2)$ at $N = 22$ also point to a sudden onset of collectivity almost immediately after $N = 20$ even for those elements for which $N = 20$ remains a viable magic number.

However, the most vivid feature of Fig. 3 is the dominance of the δS_{2n} plot by a series of sharp minima at successive neutron numbers for successive elements. These minima occur at $N = Z + 2$, and reflect the special binding known to occur [21,22] due to the Wigner effect for self-conjugate nuclei. Similar anomalies show up in another differential function of S_{2n}, namely one called δV_{pn} which reflects an average proton-neutron interaction of the last valence protons and neutrons [23]. It is interesting that this binding effect is barely visible as a small kink on the left in Fig. 3, but shows up dramatically on the right. In the $\delta E(2_1^+)$ and $\delta B(E2)$ plots, it is barely, if at all, visible. To investigate whether the special structural effects at $N = Z$ appear primarily only in binding energies or also in other observables requires much needed data on these observables as well as on $R_{4/2}$ and $\langle r^2\rangle$.

In conclusion, we showed that there are remarkable correlations among a number of differential observables in even-even nuclei spanning large regions of the nuclear chart and very different physical properties of nuclei ranging from single particle binding to nuclear sizes and collective properties

of the many-body system itself. The value of this study lies both in the correlations discovered and in the method introduced since this can have far reaching applications to a wide variety of nuclear observables far afield from those we considered here. These results open up a new way of looking at structural evolution, especially in exotic nuclei, and should be valuable in several ways. First, since data in nuclei far from stability will often be sparse (one might only know the mass and the energy of the first 2^+ state) these correlations allow estimates of the other observables. This can aid in experiments to study unknown observables far from stability and can guide theoretical expectations. Second, deviations from these correlations can be used to highlight anomalous behavior or possibly to spot data worthy of remeasurement. We illustrated this in these well-known regions with examples from intruder states in Hg and spin restrictions in the valence space in Sr, both affecting δR_{42} values. In new regions, one does not know *a priori* what anomalies may appear, but these correlations should be of use in identifying them. Third, these correlations challenge microscopic theories of structural evolution. Here we note one promising approach, the recent relativistic mean-field calculations of Ref. [24]. These currently focus on shape transition regions and exhibit almost exactly the same correlations we saw.

Our effort here has simply been to present a new method of structural analysis and to show the correlations found in well-known regions. The value of the method will, of course, be most realized in new regions. To fully exploit it, a more quantitative understanding of the quality of the correlations will be valuable. This involves some subtleties (e.g., how to deal with widely varying experimental uncertainties, even for a given observable, what degree of correlation is to be expected for various observables which are affected to different extents by structural variations, and so on) and is a subject for future thorough study.

We thank J. Billowes, K. Kreim, R. Neugart, D. Vretenar, and N. V. Zamfir for useful discussions. R.B.C. thanks the Humboldt Foundation for support. R.F.C. acknowledges the ISOLDE/CERN group for support during his research stay at CERN. Work supported by the Max-Planck Society and the US DOE under Grant No. DE-FG02-91ER-40609.

[1] National Nuclear Data Center ENSDF web program [http://www.nndc.bnl.gov/ensdf/].
[2] Center For Photonuclear Experiments Data Chart of Nucleus Shape and Size Parameters web program [http://cdfe.sinp.msu.ru/].
[3] L. Grodzins, Phys. Lett. **2**, 88 (1962).
[4] O. Scholten, F. Iachello, and A. Arima, Ann. Phys. (NY) **115**, 325 (1978).
[5] E. W. Otten, *Treatise on Heavy-Ion Science: Nuclei Far from Stability*, edited by D. A. Bromley (Plenum, New York, 1989), p. 517.
[6] M. Keim *et al.*, Nucl. Phys. A **586**, 219 (1995).
[7] F. C. Charlwood *et al.*, Phys. Lett. B **674**, 23 (2009).
[8] R. Neugart *et al.*, Hyperfine Interact. **15**, 181 (1983).
[9] P. Brix and H. Kopfermann, Rev. Mod. Phys. **30**, 517 (1958).
[10] G. D. Sprouse *et al.*, Phys. Rev. Lett. **63**, 1463 (1989).
[11] I. Angeli *et al.*, J. Phys. G **36**, 085102 (2009).
[12] A. Wolf, R. F. Casten, N. V. Zamfir, and D. S. Brenner, Phys. Rev. C **49**, 802 (1994).
[13] V. Werner *et al.*, Phys. Lett. B **527**, 55 (2002).
[14] S. Anghel, G. Cata-Danil, and N. V. Zamfir, Rom. Journ. Phys. **54**, 301 (2009).
[15] M. Simon Gerstenkorn, C. R. Acad. Sci. Paris, Ser. B **268**, 1636 (1969).
[16] I. Angeli and R. J. Lombard, Z. Phys. A **324**, 299 (1986).
[17] G. Molnar *et al.*, Nucl. Phys. A **500**, 43 (1989).
[18] R. Julin, K. Helariutta, and M. Muikku, J. Phys. G **27**, R109 (2001).
[19] Heyde *et al.*, Phys, Lett. B **155**, 303 (1985).
[20] T. Motobayashi *et al.*, Phys. Lett. B **346**, 9 (1995).
[21] J.-Y. Zhang, R. F. Casten, and D. S. Brenner, Phys. Lett. B **227**, 1 (1989).
[22] P. Van Isacker, D. D. Warner, and D. S. Brenner, Phys. Rev. Lett. **74**, 4607 (1995).
[23] R. B. Cakirli, K. Blaum, and R. F. Casten, Phys. Rev. C **82**, 061304(R) (2010).
[24] Z. P. Li *et al.*, Phys. Rev. C **79**, 054301 (2009).